NeuroImage: Clinical 30 (2021) 102610

Contents lists available at ScienceDirect

NeuroImage: Clinical

journal homepage: www.elsevier.com/locate/ynicl

High-b diffusivity of MS lesions in cervical spinal cord using ultrahigh-b DWI (UHb-DWI)

Kyle Jeong [a], Lubdha M. Shah [b], You-Jung Lee [a], Bijaya Thapa [a], Nabraj Sapkota [a], Erica Bisson [c], Noel G. Carlson [d,f,g], E.K. Jeong [a,b], John W. Rose [d,e,*]

[a] Utah Center for Advanced Imaging Research, University of Utah, Utah, USA
[b] Department of Radiology and Imaging Sciences, University of Utah, Utah, USA
[c] Department of Neurosurgery, University of Utah, Utah, USA
[d] Neuroimmunology and Neurovirology Division, Department of Neurology, University of Utah, Utah, USA
[e] Neurology Service, VA Salt Lake City Health Care System, Utah, USA
[f] GRECC, VA Salt Lake City Health Care System, Utah, USA
[g] Department of Neurobiology, University of Utah, Utah, USA

ARTICLE INFO

Keywords:
Diffusion tensor imaging, DTI
Diffusion-weighted imaging, DWI
Ultra-high B diffusion-weighted imaging
2D single-shot-DW-stimulated-EPI with reduced-FOV (2D ss-DWSTEPI-rFOV)
Cervical spinal cord
Multiple sclerosis

ABSTRACT

Purpose: The purpose of this study was to investigate UHb-rDWI signal in white matter tracts of the cervical spinal cord (CSC) and compare quantitative values between healthy control WM with both MS NAWM and MS WM lesions.

Methods: UHb-rDWI experiments were performed on (a) 7 MS patients with recently active or chronic lesions in CSC and on (b) 7 healthy control of similar age range and gender distribution to MS subjects. All MRI data were acquired using clinical 3T MRI system. Axial high-b diffusion images were acquired using 2D single-shot DW stimulated EPI with reduced FOV and a CSC-dedicated 8 channel array coil. High-b diffusion coefficient D_H was estimated by fitting the signal-b curve to a double or single-exponential function.

Results: The high-b diffusivity D_H values were measured as $(0.767 \pm 0.297) \times 10^{-3}$ mm^2/s in the posterior column lesions, averaged over 6 MS patients, and 0.587×10^{-3} mm^2/s in the corticospinal tract for another patient. The averaged D_H values of the 7 healthy volunteers from the posterior and lateral column were $(0.0312 \pm 0.0306) \times 10^{-3}$ and $(0.0505 \pm 0.0205) \times 10^{-3}$ mm^2/s, respectively. UHb-rDWI signal-b curves of the MS patients revealed to noticeably behave differently to that of the healthy controls. The patient signal-b curves decayed with greater high-b decay constants to reach lower signal intensities relative to signal-b curves of the healthy controls.

Conclusion: UHb-DWI of the CSC reveals a marked difference in signal-b-curves and D_H values in MS lesions compared to NAWM and healthy control WM. Based on physical principles, we interpret these altered observations of quantitative diffusion values to be indicative of demyelination. Further studies in animal models will be required to fully interpret UHb-DWI quantitative diffusion values during demyelination and remyelination.

1. Introduction

Spinal cord injury in multiple sclerosis (MS), due to varying degrees of demyelination and/or axonal damage, is an important cause of disability (Kremenchutzky et al., 2006). Magnetic resonance imaging (MRI) provides superb contrast and spatial resolution of the spinal cord and, therefore, is fundamental in the evaluation and monitoring of MS. Studies have shown that cord atrophy is associated with physical

Abbreviations: CSC, Cervical spinal cord; DTI, Diffusion tensor imaging; DWI, Diffusion weighted imaging; EA, Extra-axonal; FA, Fractional anisotropy; G_D, Diffusion Gradient; GM, Gray matter; D_H, High-b diffusion coefficient; IA, Intra-axonal; IAF, Intra-axonal fraction; IRB, Institutional review board; MRI, Magnetic resonance imaging; MS, Multiple Sclerosis; NAWM, Normal-Appearing White Matter; rDWI, Radial DWI; RRMS, Relapsing-remitting multiple sclerosis; T1WI, T1-weighted imaging; T2WI, T2-weighted imaging; UHb, Ultrahigh-b; UHb-rDWI, Ultrahigh-b radial DWI; WM, White matter; 2D ss-DWSTEPI-rFOV, 2D Single Shot DW Stimulated EPI with reduced FOV; 2PSM, Secondary progressive multiple sclerosis.

* Corresponding author at: Imaging and NeuroScience Center, 729 Arapeen Road, Salt Lake City, UT 84108, USA.
E-mail address: jrose@genetics.utah.edu (J.W. Rose).

https://doi.org/10.1016/j.nicl.2021.102610
Received 13 August 2020; Received in revised form 11 February 2021; Accepted 18 February 2021
Available online 8 March 2021

disability (Furby et al., 2010; Horsfield et al., 2010; Kearney et al., 2015; Losseff et al., 1996; Rocca et al., 2011). Lesion load on T_2-weighted imaging (T_2WI) has been shown to independently correlate with physical disability and is seen more often in progressive forms of MS as compared to relapsing-remitting multiple sclerosis (RRMS) (Kearney et al., 2015). However, conventional MRI sequences have limited ability to detect early stages of disease when clinical symptoms may be vague and nonspecific and also when there are diffuse abnormalities (Bot and Barkhof, 2009).

Advanced MRI techniques are currently used in exploratory studies to investigate microstructural abnormalities in the cervical spinal cord (CSC) which reflect neurodegeneration, and to develop new targets for therapeutic (Carlier and Bertoldi, 2005; Moccia et al., 2017; Moccia and Ciccarelli, 2017). These techniques include methods that study neuroaxonal integrity using DTI, myelin content using myelin water fraction (Soellinger et al., 2011) and magnetization transfer ratio (Filippi and Agosta, 2007; Pike et al., 2000; Schmierer et al., 2004; Smith et al., 2014). Among these techniques, *DTI is considered the most mature and promising for quantitative evaluation of white-matter* (Martin et al., 2016) in spinal cord. As such, there is limited correlation of these MRI findings with short- and long-term functional outcomes in MS patients. The lack of strong clinical and imaging prognostic indicators (Barkhof, 2002; Hackmack et al., 2012) contributes to poorly defined treatment pathways with outcomes that are not readily predictable. Non-invasively determining injury type and assessing areas of active remyelination and of axonal sparing will be significant in understanding the pathophysiological underpinnings of MS. Quantitative imaging biomarkers for linear characterization, monitoring disease, and measurement of therapeutic outcomes are critically needed to optimize patient care and evaluate new therapies that target remyelination.

Advanced imaging techniques such as diffusion weighted imaging (DWI) may provide such quantitative data. In DWI, the signal changes induced by the coupling between the applied diffusion gradient and the random motion of the tissue water in the background structure at specific diffusion-weighting demonstrates microscopic impediments to water movement, such as membranes, which can be used to characterize tissue structure (Le Bihan et al., 1986). DWI using ranges of b-values has shown that non-mono-exponential decay reflects diffusion restriction (Niendorf et al., 1994; Yoshiura et al., 2001) and may provide quantification of white matter (WM) structure (Ford et al., 1998; Ong et al., 2008), including axonal diameters and density (Assaf et al., 2008). The parallel orientation of the spinal cord fibers lends itself to diffusion imaging better than the brain because of a lesser degree of multiple orientations and overlapping crossing fibers that complicate not only data acquisition but also data interpretation.

In the present study, we used an ultrahigh-b radial DWI (UHb-rDWI) technique with diffusion weighted gradient (G_D) applied in the direction perpendicular to the spinal cord with diffusion weighting $b = 0 \sim 8000$ s/mm^2. We observed the signal-b curve in the UHb region ($b > 4{,}000$ s/mm^2 in CSC DWI) to provide a greater insight into CSC pathology and holds promise in distinguishing demyelination, inflammation, and axonal damage (Lee et al., 2017; Sapkota et al., 2016; Sapkota et al., 2016a; Thapa et al., 2018). This method selectively suppresses the signal contribution from the extra-axonal (EA) water at high b in order to isolate the signal of the intra-axonal (IA) water. We studied the behavior of the UHb-rDWI signal with respect to the b-values in CSC tracts with recently-active or chronic MS lesions, where water diffusion is greatly altered due to demyelination and axonal loss, relative to WM tracts in the absence of said characteristics.

2. Materials and methods

All imaging experiments were performed at a Siemens 3T MRI system (Trio, Siemens Medical Solutions, Erlangen, Germany) using 2D ss-DWSTEPI-rFOV (Sapkota et al., 2016a) and a home-developed CSC coil (Sapkota et al., 2016b). The participants were consented according to the approved protocol, which was approved by Institutional review board (IRB).

2.1. Human subjects

Five RRMS and two 2PMS patients and seven healthy controls were selected and consented to participate in this IRB approved study. All five of the RRMS patients had relapses and clinical MRI scans of the cervical spinal cord demonstrating contrast-enhancing lesions correlating with the symptoms of the relapse. Research MRI scans were performed to evaluate these recently-active lesions with UHb-DWI. One patient (MS1: 48y/M) had a lesion in right lateral column and four patients had lesions in the posterior columns (MS2: 22y/F, MS3: 48y/F, MS4: 36y/F, MS5: 53y/F). In addition, chronic posterior column lesions in two patients with 2PMS were studied (MS6: 56y/M, MS7: 59y/M).

All 5 of the relapsing and remitting patients received corticosteroid therapy: 4 with methylprednisolone dosage of 1000 mg intravenously for 3 days and 1 with prednisone 80 mg/per day for several days with rapid taper due to side effects, while the 2PMS patients were not treated with corticosteroids prior to the research imaging. Table 1 lists the type, location and level of the lesions, the measured D_H values of the lesion and NAWM, as well as age and gender of the 7 patients. The control group data included four healthy normal subjects (27/F, 56/F, 34/M, 39/M) from our previous reports (21, 22) and additional three normal subjects (28/F, 27/F, 31/F).

2.2. MS1

A 48-year-old male with a 14-year history of RRMS, presented with new onset of right lower extremity paresthesias and weakness and associated unsteady ambulation. The T2WI revealed an intramedullary lesion at the C3-C4 level. He was given methylprednisolone 1000 mg IV each day for 3 days after day 11, and the symptoms resolved with improved strength and ambulation at day 83. Research MRI was performed 11 days after the clinical scan.

2.3. MS2

A 22-year-old female with 4-year history of RRMS, presented acutely with impaired balance, ambulation, and vibratory sensation. The initial clinical MRI revealed a new contrast-enhancing lesion in the posterior spinal cord at the C2-C3 level. The patient underwent treatment with oral prednisone for several days with rapid taper and recovered clinically over 4 months. Research MRI was performed 33 days after the clinical scan.

2.4. MS3

A 48-year-old female with RRMS experienced a 2-week progression of impaired sensation ascending from the feet into the arms. Neurologic evaluation demonstrated Lhermitte's sign, mild paraparesis, impaired vibratory sensation in the lower extremities with a wide based gait, unsteady tandem gait, and a positive Romberg test. The patient had not been on immunotherapy at the time of the relapse. Clinical MRI of the cervical spinal cord revealed a new contrast enhancing lesion in the posterior columns at the C2 level. Patient was treated with IV methylprednisolone. Research MRI was performed 15 days after the clinical scan.

2.5. MS4

A 36-year-old female with RRMS had a severe relapse evolving over 3 days with new onset of neck pain, Lhermitte's sign, reduced vibration sensation in all extremities, increased right hemiparesis and right hemihypesthesia to touch and temperature. Her ambulation was markedly impaired and she had become largely wheel chair dependent. IV

Table 1
Measured D_H values of 7 MS patients. For each patient, D_H values at the lesion and NAWM are estimated. The mean D_H values of healthy controls are estimated as $(0.0505 \pm 0.0306) \times 10^{-3}$ and $(0.0312 \pm 0.0205) \times 10^{-3}$ mm^2/s for lateral corticospinal tract and posterior sensory tract at the C3-C4 level, respectively. Mean FA values of 7 healthy subjects are 0.762 ± 0.050 and 0.677 ± 0.042 at lateral corticospinal tract and dorsal sensory columns, respectively. (CS: corticospinal tract, PC: posterior column). MS4 had a reactivation of a lesion.

Subject	Type/Age/Gender	Lesion Type	Location/Level	Lesion		NAWM	
				$D_H \times 10^{-3}$ mm^2/s	FA	$D_H \times 10^{-3}$ mm^2/s	FA
MS1	RRMS/48/M	Recently active	CS/C3-4	0.597	0.620	0.126	0.735
MS2	RRMS/22/F	Recently active	PC/C2	0.856	0.539	0.092	0.630
MS3	RRMS/48/F	Recently active	PC/C2	0.374	0.435	0.179	0.562
MS4	RRMS/36/F	Recently active	PC/C2-C3	0.990	0.394	0.139	0.613
MS5	RRMS/53/F	Recently active	PC/C2-3	0.430	0.482	0.025	0.537
MS6	2PMS/56/M	Chronic	PC/C2	1.096	0.430	0.354	0.580
MS7	2PMS/59/M	Chronic	PC/C2-C3 & C3-C4	0.853	0.540	0.445	0.687
MS mean				0.742	0.484	0.194	0.614
MS stdDev				0.278	0.082	0.150	0.073

methylprednisolone therapy was effective, and she regained independent ambulation over the subsequent 21 days. Clinical MRI at the time of the relapse revealed a C2-C3 cervical spinal cord lesion with contrast enhancement involving the right lateral and posterior columns. Research MRI scan was performed 37 days after the onset of symptoms.

2.6. MS5

A 53-year-old female with RRMS had a relapse with onset of paraesthesias in the left arm and hand while non-compliant with medication. Clinical MRI scan of the cervical spinal cord revealed an actively enhancing lesion involving the posterior columns and central cord at the C2-3 level. IV methylprednisolone was administered for 3 days. She had an initial improvement and then continued to recover slowly over 6 months. Research MRI was performed 84 days after the clinical scan.

2.7. MS6

A 56-year-old male with 2PMS had a longstanding and stable lesion involving the posterior columns, more prominently on the left, the C2 level. This lesion appeared unchanged on 8 serial clinical MRI scans from 2002 to the present. Research MRI was performed 44 days after the most recent clinical scan.

2.8. MS7

A 59-year-old male with 2PMS has longstanding and stable lesions at the C2 level in the right posterior and lateral columns and a second lesion at C3-4 involving the posterior columns. These lesions remained on 5 serial clinical MRIs from 2002 to the present. Research MRI was performed 123 days after the most recent clinical scan.

2.9. MRI protocol

Subject was positioned within the RF coil, of which the cervical portion of the neck is as straight as possible. After a 3-plane scout imaging, T_2WI were acquired in both coronal and sagittal planes for the UHb-rDWI experiment in axial plane. Axial T_2WI were acquired with TR 4 s, TE 95 ms, and acquisition resolution $0.68 \times 0.55 \times 4.0$ mm^3 using a turbo spin-echo (TSE). To minimize the geometrical distortion, advanced shimming was performed on the imaging volume, and UHb-rDWI experiment was conducted in the axial plane using the 2D ss-DWSTEPI-rFOV pulse sequence and an 8-channel CSC dedicated array coil (Sapkota et al., 2016b), using TR/TE = 3 s/64 ms, 128×44 mm^2 imaging FOV, 8 averages, 21 slices with $1.0 \times 1.0 \times 4.0$ mm^3 voxel dimension, and 7b-values ($142 \sim 7348$ s/m^2) along the left–right direction. b-value was varied by varying mixing time TM (time interval between the 2nd and 3rd 90° RF pulses) with 9, 85, 161, 237, 313, 389, 465 ms, which correspond seven b-values of 570, 1700, 2830, 3960, 5090, 6220, 7350 s/mm^2, respectively, while maintaining a constant duration $\delta = 12$ ms and amplitude $G_D = 38$ mT/m of the diffusion gradient. The data acquisition time for UHb-rDWI was about 7 min. An additional set of b_o images without diffusion weighting gradient was obtained corresponding to each TM for correcting T_1 decay during TM. For the same slice location as those UHb-DWI, DTI experiment was performed with b = 0 and 500 s/mm^2 for 12 non-colinear diffusion-encoding directions for diffusion tensor MRI using TR 4 s and spatial resolution $1.0 \times 1.0 \times 4.0$ mm^3.

2.10. Image processing

All DICOM images were post-processed using a homemade software written in Python 3.x language. The signal equation for diffusion-weighted images (S_b) and b_o images (S_{bo}) incorporating the diffusion and T_1 decay effects are:

$$S_b = \left(S_0^L e^{-bD_L} + S_o^H e^{-bD_H}\right) e^{-TM/T_1} \quad (2)$$

$$S_{b0} = S_o e^{-TM/T_1}, S_o = \left(S_o^{IA} + S_o^{EA}\right) \quad (3)$$

where S_o is the signal intensity without T_1 and diffusion decay, and D_L and D_H are apparent diffusion coefficients at low- and high-b regions, or equivalently fast and slow-varying components in two compartment model, respectively. The diffusion-prepared longitudinal magnetization undergoes both diffusion and T_1 decay during the duration between the second and third 90° RF pulses, while b_o signal undergoes only T_1 decay. After subtracting the background noise mean, T_1 was calculated by fitting the signals of b_0 images to a single-exponential function in pixel-by-pixel as in eq. [3], then used to remove the T_1 decay in the UHb-DWI signals. The pure diffusion signal is obtained by removing T_1 decay term in eq. [2]. The normalized DW signals were fitted to both a bi-exponential and mono-exponential plus constant function (Sapkota et al., 2016), and the fit with smaller χ^2 is kept.

3. Results

The UHb-rDWI results reveal that the signal measured in the UHb region (b > 4,000 s/mm^2) from the healthy cord is predominantly from the restricted IA space in healthy CSC (Fig. 1), and the curves generated by UHb-rDWI are consistent with those predicted from our previous investigations in the ex-vivo cord. Fig. 1b illustrates the typical signal-b curves of a square-shaped 9-pixel square ROI (36 mm^3) in UHb-rDWI data at two contra-lateral fiber tracts in the healthy human CSC. The signal intensity graphs show that UHb-rDWI is consistent for the spinal cord tracts from the C1 to the C4 vertebral levels, as we have previously reported (Thapa et al., 2018). Our results also demonstrate the consistency of UHb-rDWI between the contralateral tracts in the CSC, including the lateral funiculi and the posterior columns. Furthermore,

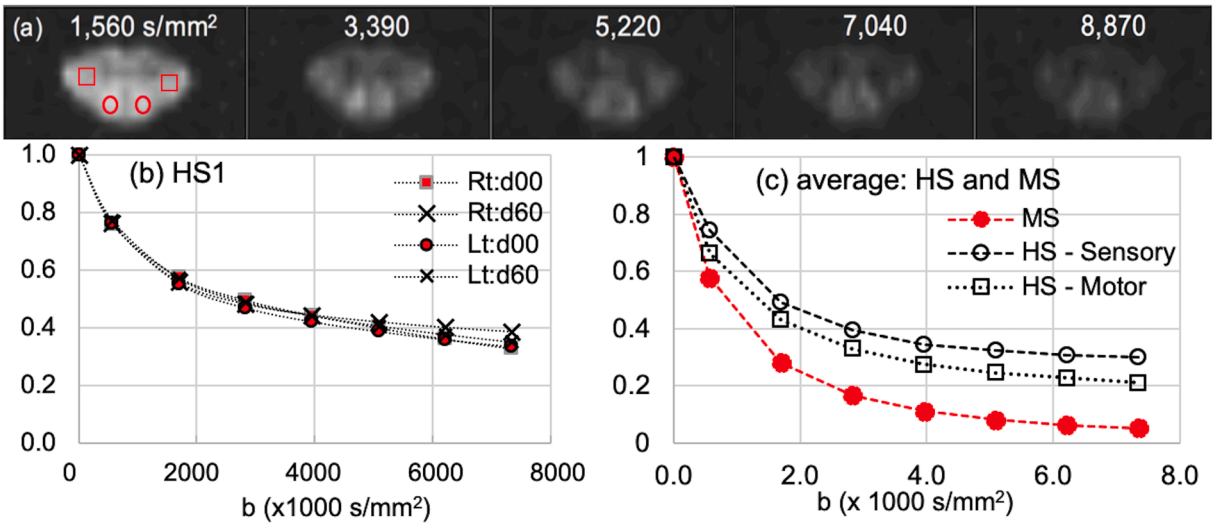

Fig. 1. (a) Series of DW images with b = 1,560 ~ 8,870 s/mm^2 and diffusion gradient $\vec{G}_D$ applied along the left–right direction, perpendicular to the cord fiber. (b) Typical signal-b curves of UHb-DWI of two contralateral ROIs at corticospinal (□) and dorsal sensory (O) tracts (Rt: right lateral funiculus, Lt: left lateral funiculus) and in a healthy human CSC at the C3-C4 level 60 days apart. The signal-b curves at the two different time points and regions indicate the high reproducibility of the UHb-DWI technique. (c) Signal-b curves of posterior sensory tract (O) and corticospinal (or motor) tract (□) averaged over two ROIs (left and right) of 7 healthy subjects, and lesion ROIs of all MS subjects (●).

the UHb-rDWI findings did not vary in the 60-day interval (Fig. 1b), also presented in our previous report (Thapa et al., 2018).

Plots in Fig. 1c present the averaged signal intensities of two contralateral (left and right) ROIs of 7 healthy subjects at corticospinal tract (□) and dorsal sensory tract (o). D_H values of healthy controls are measured on C2-C3, C4, and C5 vertebral levels at two contralateral ROIs of the lateral funiculi (corticospinal tract) and two contralateral ROIs of the posterior column (sensory tracts). The solid circles (•) in Fig. 1c indicate the UHb-rDWI data of MS lesions of all patients. The mean D_H values of healthy controls for lateral corticospinal tract and posterior sensory tract at the C3-C4 level are estimated as $(0.0505 \pm 0.0306) \times 10^{-3}$ and $(0.0312 \pm 0.0205) \times 10^{-3}$ mm^2/s, respectively. D_H values at the recently-active lesions and NAWM, averaged over the first research images of 7 MS patients, were estimated as $(0.742 \pm 0.279) \times 10^{-3}$ mm^2/s and $(0.194 \pm 0.150) \times 10^{-3}$ mm^2/s, which are significantly larger than those of healthy subjects (Thapa et al., 2018). Note that the average signal-b curve of all the recently-active MS lesions, represented by the open-circle (o) in Fig. 1c, fits the best to a single-exponential function, which indicates a rapid exchange of the water molecules between IA and EA spaces. Fractional-anisotropy (FA) values were estimated in each MS subject (listed in Table 1) and average FA values are as 0.485 ± 0.082 and 0.614 ± 0.073 at the lesion and NAWM ROIs, respectively. As references, the mean FA values of 7 healthy subject which are averaged for two ROIs at left and right columns at C3-C4 level, are 0.762 ± 0.050 and 0.677 ± 0.042 at the lateral corticospinal tract and dorsal columns, respectively.

At the time of relapse for patient MS1, clinical MRI demonstrated a new enhancing lesion (L1 in Fig. 2a) in the right lateral funiculus at the C3-C4 level on Gd-T1WI, which corresponds to T_2 hyperintense lesion. This lesion also demonstrated decreased fractional anisotropy (FA) (red circle in Fig. 2d). Note that the decreased FA may be caused by increased concentration of extra-cellular water (edema) and/or increased water exchange at the myelin sheath (demyelination).

Fig. 3 compares the lesion and NAWM of patient MS1 to the healthy subjects in regards to the UHb-rDWI signal-b curves and the D_H values. The arrow in b = 7350 s/mm^2 image indicates the lesion, of which DWI signal is decayed to the background noise level. The DWIs of b = 3960 s/mm^2 in Fig. 3b present pixels (red dots) included in ROIs at the lesion and NAWM that is located 1.5 cm above the lesion toward the brain. Signal-b curves of the lesion (■) and NAWM (□) of MS1, as well as that of the healthy subjects, at the aforementioned ROIs are shown in Fig. 3c. Signal-b of the lesion shows a prominent decaying pattern compared to that for the NAWM. The abnormal lateral funiculus UHb-rDWI was observed at multiple levels (C2-C4). Interestingly, UHb-rDWI signal-b curve of the NAWM behave close to that of the normal subject. The high-b diffusion coefficient D_H in the lesion, NAWM, and healthy subjects are illustrated in Fig. 3d. The measured D_H values are 0.597×10^{-3} mm^2/s, 0.126×10^{-3} mm^2/s, and 0.056×10^{-3} mm^2/s for the lesion, NAWM, and the averaged signal-b curves at the corticospinal tract of healthy CSCs, respectively. The individual data of four healthy CSCs have been presented with more detail in our previous report (Thapa et al., 2018).

On the initial clinical MRI of patient MS2, the axial T2WI (Fig. 4a)

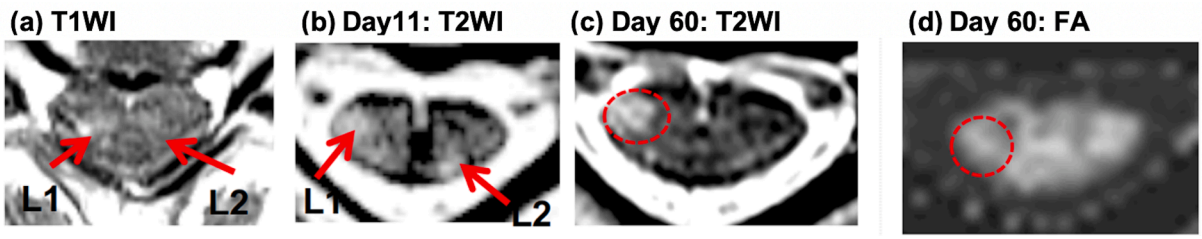

Fig. 2. Patient MS1: (a) Axial Gd-enhanced T1WI at day 1 demonstrates an enhancing lesion in the right lateral funiculus. T2WI at day 11 (b) and at day 60 (c) reveal corresponding T2 hyperintense lesions in the right lateral funiculus. The lesion is smaller and more well defined at day 60 as compared to day 11. (b) A second non-enhancing T2 hyperintense lesion in the left posterior column corresponds to an older lesion (L2). Fractional anisotropy (FA) fibermap at day 60 (d) shows reduced FA values in the right lateral funiculus lesion within the circle as compared to the contralateral region.

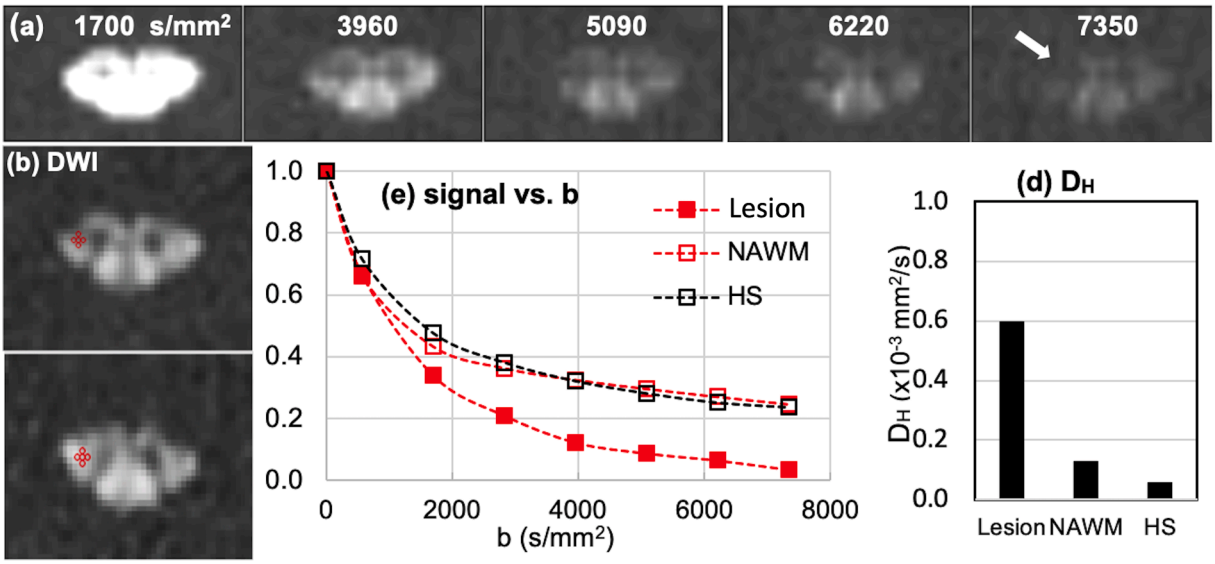

Fig. 3. MS1: (a) DWIs of b = 1700 ~ 7350 s/mm^2 of the lesion slice and (b) ROIs at lesion and NAWM slice, 1.5 cm above the lesion toward the brain, and (c) signal-b curves of the recently-active lesion (■) and NAWM (●), and averaged data (□) at the corticospinal tract of seven healthy subjects, and (d) mean values of high-b diffusion coefficient D_H at the lesion, NAWM, and the healthy CSCs at the corticospinal tract.

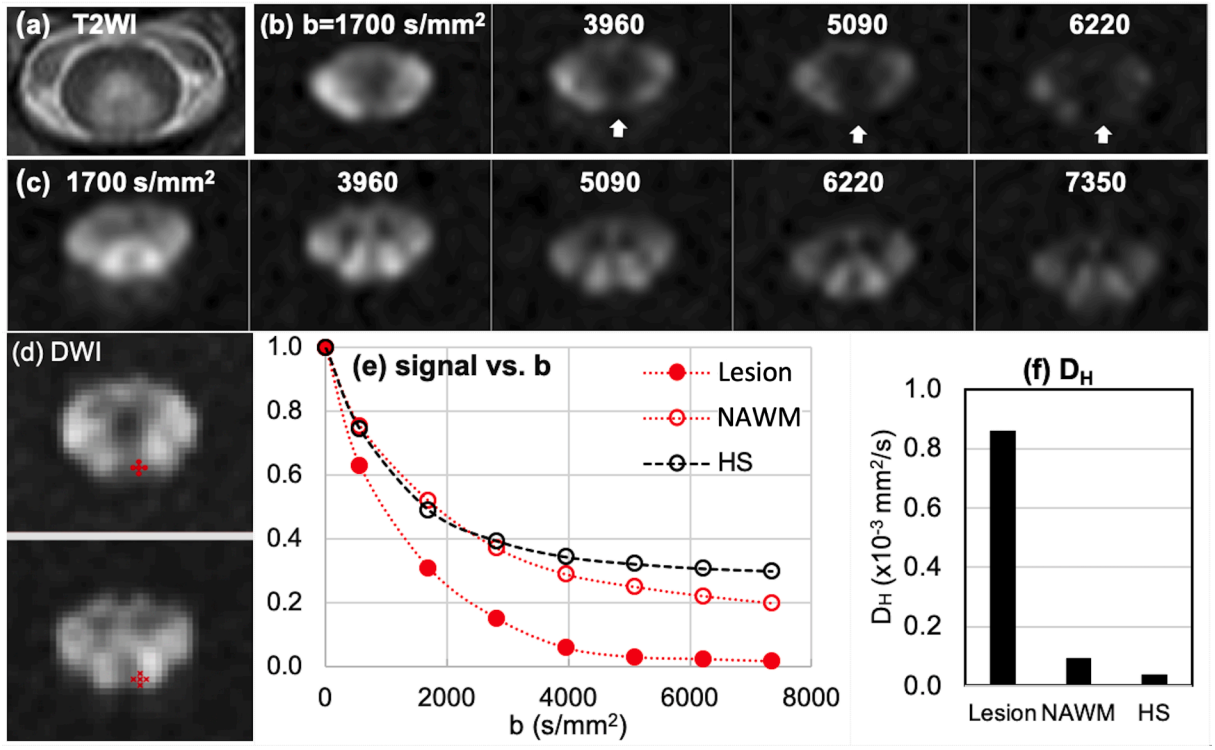

Fig. 4. MS2: (a) T2WI, (b, c) DWIs of b = 1700 ~ 7350 s/mm^2 of the lesion slice and NAWM slice, 1.5 cm below the lesion away from the brain, (d) ROIs on lesion (top) and NAWM (bottom), (e) signal-b curves of the recently-active lesion (●) and NAWM (O), and averaged data (O) at the posterior column of seven healthy subjects, and (f) mean values of high-b diffusion coefficient D_H at the lesion, NAWM, and the healthy CSCs at the corticospinal tract. White vertical arrows in (a) indicate lesion with rapidly decaying signal.

showed an ovoid hyperintense lesion in the posterior spinal cord at the C2 level; indicating increased parenchymal water content. In Fig. 4b and c, DWIs of b = 1700 ~ 7350 s/mm^2 of the lesion slice and NAWM slice, 1.5 cm below the lesion away from the brain show a lesion (Fig. 4b) with rapidly decaying signal. DWI signal at the lesion is almost suppressed down to noise level at b = 5090 s/mm^2, as indicated in Fig. 4c, while those remain high on NAWM tracts in the lesion slice and other slice, 1.5 cm below. Fig. 4e illustrates the distinctively different signal-b curve behavior of the MS2 lesion (●) compared to that of the healthy subjects (**O**). The UHb-rDWI signal of the NAWM is plotted with the open red circle (O) for reference. The measured D_H values (plotted in Fig. 4f) are 0.856 × 10^{-3}, 0.092 × 10^{-3}, and 0.035 × 10^{-3} mm^2/s for the lesion, NAWM, and the averaged healthy CSCs, respectively. NAWM had seemingly comparable signal intensity throughout different b-values to

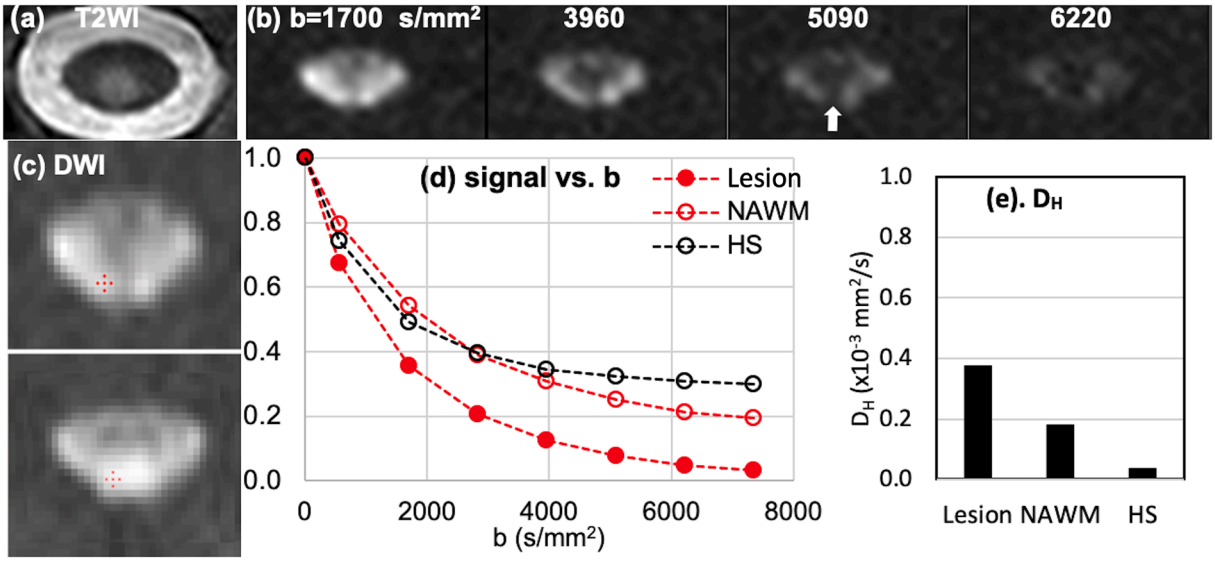

Fig. 5. MS3: (a) T2WI and (b) DWIs of lesion slice, (c) ROIs on lesion (top) and NAWM (bottom), (d) signal-b curves of the recently-active lesion (●) and NAWM (O), and averaged data at the posterior column of seven healthy subjects (O), and (e) mean values of high-b diffusion coefficient D_H at the lesion, NAWM, and the healthy CSCs at the posterior column. White vertical arrow on (b) indicates signal void at the posterior column.

that the healthy subjects. However, the D_H of NAWM is much larger than average D_H of the healthy subjects.

Patient MS3 has a recently-active lesion in posterior column at C2 level. T2WI in Fig. 5a shows this recently-active lesion centered at the dorsal column, and Fig. 5b and c indicate UHb-rDWIs with b-value up to 6220 s/mm^2 and ROIs at the lesion and NAWM slice, respectively. The NAWM slice is located 1.5 cm below the lesion slice away from the brain. ROI of the NAWM slice is selected at the same ascending tract as the lesion ROI. The UHb-rDWI signals of the lesion (●) and NAWM (**O**) are plotted with respect the b-value in Fig. 5d. Both lesion and NAWM signal-b curves, particularly lesion signal, deviate from that of healthy cord (O) with greatly elevated decay constant D_H. D_H values were estimated as 0.374×10^{-3} and 0.179×10^{-3} mm^2/s for the lesion and NAWM ROIs, respectively.

UHb-DWI data of all other four MS subjects (MS4, MS5, MS6, and MS7), of which lesions are located in the posterior column, were post-processed as for MS1, MS2 and MS3. We analyzed signal-b curves and measured D_H values at the lesion and an NAWM ROIs. Signal-b curves of lesion in these MS subjects deviated from the healthy reference data, similar to those of MS1, MS2, and MS3, as illustrated in Figs. 3c, 4e, and 5d. D_H values of ROIs at the lesion are an order of magnitude larger than the average D_H of the posterior column in healthy cord, as listed in Table 1.

4. Discussion

Advanced MRI techniques, such as UHb-rDWI, may have the potential for demonstrating quantitative evidence of axonal injury, demyelination, and remyelination in MS as it allows detailed microstructural evaluation. Not only is there increased GM-WM contrast at higher b values because of the non-mono-exponential signal decay in WM (Rangwala et al., 2013; Yoshiura et al., 2001), the signal-b curve of UHb-rDWI can also be used to estimate water exchange rate between the IA and EA spaces. Water molecules, which are confined within a restricted space such as in the healthy myelinated axon, are expected to show little decay in their UHb-DWI signal with respect to the diffusion weighting applied perpendicular to the axonal fiber direction. The measured signal-b curve is predicted to follow a double-exponential decay function with a fast decay in low-b and slow decay in high-b regions, which are dominated by the signals from EA and IA spaces, respectively. The slow decay of the IA water in healthy cord is caused by the water-exchange at the interface of myelin and the node of Ràvnier.

In addition, UHb-DWI can be utilized to quantify axonal damage. Axonal damage may be assessed by applying the UHb diffusion gradients along the axial direction. The hindrances in the axial diffusion of the IA water is increased in lesions, assuming that the IA space may not be as straight as in the healthy CSC (Budde and Frank, 2010). The measured data for UHb-rDWI, including the high-b diffusion coefficient D_H, provides much deeper insight about the microscopic environment in the WM in addition to λ_r, λ_a, FA.

For the UHb-rDWI, the CSC WM may be compartmentalized into (1) "*restricted*" IA space where water cannot move more than the diameter of the axon and (2) all other "*mobile*" EA space where water can move through the hindered boundaries, including the membranes. At the microstructural level in a healthy spinal cord, the movement IA water molecules is highly restricted by the hydrophobic myelin sheath, whose many lipid-bilayers confine charged ion particles within the IA space, except at the nodes of Ranvier. The maximum distance that IA water molecules can travel perpendicular to the nerve direction is the mean diameter of the axons, of which peak size was reported as 1.2 μm (Lovas et al., 2000). At sufficiently high diffusion-weighting (b > ~ 4000 s/mm^2 in a clinical MRI system) and with TE longer than 50 ms, which is >5*T_2, we observed that the DWI signal from "*mobile*" water protons in EA and myelin space was completely suppressed to background noise level, which leaves only the signal contributed from IA water.

In early demyelination, there may be local infiltration of immune cells and an increased exchange rate is anticipated with an increase in the high-b diffusion coefficient D_H. As the molecular diffusivities of these cells differ from other spaces, this can influence the signal behavior of the low-b and axial DWI, but UHb-rDWI is not affected. At a low percentage of demyelination, EA water molecules have a non-zero probability to enter into the IA space; therefore, the signal at low-b region decays slower.

UHb-rDWI has the advantage of reflecting changes in the EA and IA spaces at lower values and only the IA space at higher b values. In the normal CSC, the signal from the EA space decayed while that from the IA space was constant, regardless of the b values. In the RRMS patients, the regions of active lesions revealed marked decrease in signal intensities in the high-b zone. The applied radial diffusion gradient does not create noticeable phase dispersion for the spins in water molecules restricted in the IA space whose motion along radial direction is limited by axonal diameter. However, this applied radial diffusion gradient does create a

phase dispersion for the spins in mobile water molecules in EA space. Demyelinating lesions enable the exchange of water molecules between IA and EA spaces, which results in the marked signal decay in the IA space. In RRMS patients, UHb-rDWI revealed the extent of lesions in the CSC during the active episode and over the course of the recovery period. The rapid signal decay at high b region in the MS lesions and gradual approach of the signal-b curve at the lesion toward that of the normal control may potentially be indicators for demyelination with axonal sparring and remyelination, respectively.

The UHb-rDWI technique also raises possibility of interrogating the CSC microstructure in normal and disease states in correlation with clinical status. Abnormalities in diffusivity in the corticospinal tracts and in the posterior columns have been shown to be associated with locomotor disability and sensory impairment (Naismith et al., 2013), which was seen in our patients MS1 ~ MS7. Demyelination and axonal permeability may be the two primary factors affecting the signal-b behavior. The plateau of the signal-b curve may represent axonal density, which decreases with inflammation.

These results illustrate the potential of UHb-rDWI to detect the evolution of MS lesions from active demyelination with axonal sparing to the axonal preservation with remyelination. Although Gd-enhancement with increased diffusivity is typically interpreted to reflect an active lesion, a portion of demyelinating lesions may have early restricted diffusivity without enhancement. This may reflect increased EA space and cellularity with varying degrees of blood–brain/cord barrier breakdown (Preziosa et al., 2016; Rovira et al., 2002). Because conventional MRI of such acute lesions may be subtle and may not enhance (Grossman and McGowan, 1998; Thompson et al., 1991), particularly due to technical changes in imaging spinal cords, the UHb-rDWI will be helpful in detecting early changes in the EA and IA spaces and in understanding the microstructural changes. Furthermore, conventional MRI cannot grade the extend of tissue injury within macroscopic lesions or detect and quantify the occult damage known to occur in normal-appearing cord of MS patients (Bergers et al., 2002). Additionally, although contrast-enhanced MRI may appear to be a sensitive method for detecting active MS lesions, lesion activity should not be equated with enhancement; more activity is present than those that are defined by enhancement (He et al., 2001). There are potential implications for the higher D_H values for NAWM for two 2PMS patients (MS6 and MS7) indicative of greater demyelination than in the RRMS patients and the subject of future investigations.

This study has a few limitations. UHb-rDWI is measured using an in house-developed pulse sequence 2D ss-DWSTEPI-rFOV for optimal SNR at ultrahigh b DWI. The optimal signal-to-noise ratio with the highest contrast and spatial resolution is achieved using our self-made CSC RF coil (Sapkota et al., 2016b). Although the 7-minute sequence is feasible in the clinical realm, it does require good patient cooperation during the imaging. Our experience has revealed that the best imaging results are in the upper CSC where the spinal alignment is straight; however, we can compensate for curvature in the cord by regional adjustments in the imaging. With normal cervical lordosis, there can be field inhomogeneity with distortion in the mid and lower cervical spine. Therefore, adjustments must be made to accommodate for the cervical spine curvature below C4.

Although our studies were conducted with a limited number of MS patients, our promising results show that signal at higher b values is from only the IA space. The concordance of the UHb-rDWI patterns with clinical findings (Table 1) raises speculations of the histological correlations of demyelination and axonal injury. Definitive histopathologic correlation with UHb-rDWI in animal models will be our next steps.

5. Conclusion

The reliability of UHb-rDWI to show demyelination is illustrated by the abnormal quantitative diffusion values in the MS patients relative to the normal subjects. In this preliminary study of 7 MS subjects, the high-b diffusivity D_H was elevated an order of magnitude compared with D_H in healthy cords. We believe D_H may potentially be a reliable biomarker to evaluate the degree of demyelination in MS spinal cord, which may become a powerful method to evaluate active and chronic lesions. In ongoing investigations, we will validate UHb-DWI quantitative diffusion values during demyelination and remyelination in longitudinal studies in MS as well as animal models.

CRediT authorship contribution statement

Kyle Jeong: Conceptualization, Methodology, Software, Writing - original draft. **Lubdha M. Shah:** Formal analysis, Writing - review & editing. **You-Jung Lee:** Investigation, Resources. **Bijaya Thapa:** Investigation. **Nabraj Sapkota:** Investigation, Methodology. **Erica Bisson:** Formal analysis. **Noel G. Carlson:** Formal analysis, Writing - review & editing. **E.K. Jeong:** Conceptualization, Supervision, Methodology, Software, Writing - review & editing, Funding acquisition, Project administration. **John W. Rose:** Validation, Writing - review & editing, Funding acquisition, Project administration.

Acknowledgements

Our investigations were funded by NMSS RG 5233-A-2 and NIH R56R01 NS106097-01A1 (EKJ) and the coil development was funded by VA merit review grant (JWR). These investigations utilized a 3T Research MRI system donated by the Cumming Foundation. The investigators greatly appreciate support for this study from Alice and Kevin Steiner.

Data availability statement

Human participants of this study did not consent for their data to be publicly shared. Therefore, the presented data is not available to be shared.

References

Assaf, Y., Blumenfeld-Katzir, T., Yovel, Y., Basser, P.J., 2008. AxCaliber: a method for measuring axon diameter distribution from diffusion MRI. Magn. Reason. Med. 59 (6), 1347–1354. https://doi.org/10.1002/(ISSN)1522-259410.1002/mrm.v59:610.1002/mrm.21577.

Barkhof, F., 2002. The clinico-radiological paradox in multiple sclerosis revisited. Curr. Opin. Neurol. 15 (3), 239–245. https://doi.org/10.1097/00019052-200206000-00003.

Bergers, E., Bot, J.C.J., van der Valk, P., Castelijns, J.A., Lycklama A Nijeholt, G.J., Kamphorst, W., Polman, C.H., Blezer, E.L.A., Nicolay, K., Ravid, R., Barkhof, F., 2002. Diffuse signal abnormalities in the spinal cord in multiple sclerosis: direct postmortem in situ magnetic resonance imaging correlated with in vitro high-resolution magnetic resonance imaging and histopathology. Ann. Neurol. 51 (5), 652–656. https://doi.org/10.1002/(ISSN)1531-824910.1002/ana.v51:510.1002/ana.10170.

Bot, J.CJ., Barkhof, F., 2009. Spinal-cord MRI in multiple sclerosis: conventional and nonconventional MR techniques. Neuroimaging Clin. N. Am. 19 (1), 81–99. https://doi.org/10.1016/j.nic.2008.09.005.

Budde, M.D., Frank, J.A., 2010. Neurite beading is sufficient to decrease the apparent diffusion coefficient after ischemic stroke. Proc. Natl. Acad. Sci. 107 (32), 14472–14477. https://doi.org/10.1073/pnas.1004841107.

Carlier, P.G., Bertoldi, D., 2005. In vivo functional NMR imaging of resistance artery control. Am. J. Physiol. Heart Circ. Physiol. 288 (3), H1028–H1036. https://doi.org/10.1152/ajpheart.00780.2004.

Filippi, M., Agosta, F., 2007. Magnetization transfer MRI in multiple sclerosis. J. Neuroimaging.

Ford, J.C., Hackney, D.B., Lavi, E., Phillips, M., Patel, U., 1998. Dependence of apparent diffusion coefficients on axonal spacing, membrane permeability, and diffusion time in spinal cord white matter. J. Magn. Reson. Imaging 8 (4), 775–782. https://doi.org/10.1002/(ISSN)1522-258610.1002/jmri.v8:410.1002/jmri.1880080405.

Furby, J., Hayton, T., Altmann, D., Brenner, R., Chataway, J., Smith, K.J., Miller, D.H., Kapoor, R., 2010. A longitudinal study of MRI-detected atrophy in secondary progressive multiple sclerosis. J. Neurol. 257 (9), 1508–1516. https://doi.org/10.1007/s00415-010-5563-y.

Grossman, R.I., McGowan, J.C., 1998. Perspectives on multiple sclerosis. Am. J. Neuroradiol. 19, 1251–1265.

Hackmack, K., Weygandt, M., Wuerfel, J., Pfueller, C.F., Bellmann-Strobl, J., Paul, F., Haynes, J.-D., 2012. Can we overcome the “clinico-radiological paradox” in multiple

sclerosis? J. Neurol. 259 (10), 2151–2160. https://doi.org/10.1007/s00415-012-6475-9.
He, J., Grossman, R.I., Ge, Y., Mannon, L.J., 2001. Enhancing patterns in multiple sclerosis: evolution and persistence. Am. J. Neuroradiol. 22, 664–669.
Horsfield, M.A., Sala, S., Neema, M., Absinta, M., Bakshi, A., Sormani, M.P., Rocca, M.A., Bakshi, R., Filippi, M., 2010. Rapid semi-automatic segmentation of the spinal cord from magnetic resonance images: application in multiple sclerosis. Neuroimage 50 (2), 446–455. https://doi.org/10.1016/j.neuroimage.2009.12.121.
Kearney, H., Schneider, T., Yiannakas, M.C., Altmann, D.R., Wheeler-Kingshott, C.A.M., Ciccarelli, O., Miller, D.H., 2015. Spinal cord grey matter abnormalities are associated with secondary progression and physical disability in multiple sclerosis. J. Neurol. Neurosurg. Psychiatry 86 (6), 608–614. https://doi.org/10.1136/jnnp-2014-308241.
Kremenchutzky, M., Rice, G.P.A., Baskerville, J., Wingerchuk, D.M., Ebers, G.C., 2006. The natural history of multiple sclerosis: a geographically based study 9: observations on the progressive phase of the disease. Brain 129, 584–594. https://doi.org/10.1093/brain/awh721.
Le Bihan, D., Breton, E., Lallemand, D., Grenier, P., Cabanis, E., Laval-Jeantet, M., 1986. MR imaging of intravoxel incoherent motions: application to diffusion and perfusion in neurologic disorders. Radiology 161 (2), 401–407. https://doi.org/10.1148/radiology.161.2.3763909.
Lee, Y.J., B.Thapa, Sapkota, N., Kim, E.J., Shah, L.M., Rose, J.W., E.K. Jeong, 2017. Ultra- high-b diffusion imaging of cervical spinal cord in multiple sclerosis. In: 2017 Annual Meeting of ISMRM. Honolulu, HI, USA, p. 2561.
Losseff, N.A., Webb, S.L., O'Riordan, J.I., Page, R., Wang, L., Barker, G.J., Tofts, P.S., McDonald, W.I., Miller, D.H., Thompson, A.J., 1996. Spinal cord atrophy and disability in multiple sclerosis. A new reproducible and sensitive MRI method with potential to monitor disease progression. Brain 119 (3), 701–708. https://doi.org/10.1093/brain/119.3.701.
Lovas, G., Szilagyi, N., Majtenyi, K., Palkovits, M., Komoly, S., 2000. Axonal changes in chronic demyelinated cervical spinal cord plaques. Brain Pt 123 (2), 308–317. https://doi.org/10.1093/brain/123.2.308.
Martin, A.R., Aleksanderek, I., Cohen-Adad, J., Tarmohamed, Z., Tetreault, L., Smith, N., Cadotte, D.W., Crawley, A., Ginsberg, H., Mikulis, D.J., Fehlings, M.G., 2016. Translating state-of-the-art spinal cord MRI techniques to clinical use: a systematic review of clinical studies utilizing DTI, MT, MWF, MRS, and fMRI. NeuroImage Clin.
Moccia, M., Ciccarelli, O., 2017. Molecular and metabolic imaging in multiple sclerosis. Neuroimaging Clin. N. Am. https://doi.org/10.1016/j.nic.2016.12.005.
Moccia, M., de Stefano, N., Barkhof, F., 2017. Imaging outcome measures for progressive multiple sclerosis trials. Mult. Scler. https://doi.org/10.1177/1352458517729456.
Naismith, R.T., Xu, J., Klawiter, E.C., Lancia, S., Tutlam, N.T., Wagner, J.M., Qian, P., Trinkaus, K., Song, S.-K., Cross, A.H., 2013. Spinal cord tract diffusion tensor imaging reveals disability substrate in demyelinating disease. Neurology 80 (24), 2201–2209. https://doi.org/10.1212/WNL.0b013e318296e8f1.
Niendorf, T., Norris, D.G., Leibfritz, D., 1994. Detection of apparent restricted diffusion in healthy rat brain at short diffusion times. Magn. Reson. Med. 32 (5), 672–677. https://doi.org/10.1002/(ISSN)1522-259410.1002/mrm.v32:510.1002/mrm.1910320520.
Ong, H.H., Wright, A.C., Wehrli, S.L., Souza, A., Schwartz, E.D., Hwang, S.N., Wehrli, F. W., 2008. Indirect measurement of regional axon diameter in excised mouse spinal cord with q-space imaging: simulation and experimental studies. Neuroimage 40 (4), 1619–1632. https://doi.org/10.1016/j.neuroimage.2008.01.017.
Pike, G.B., De Stefano, N., Narayanan, S., Worsley, K.J., Pelletier, D., Francis, G.S., Antel, J.P., Arnold, D.L., 2000. Multiple sclerosis: magnetization transfer MR imaging of white matter before lesion appearance on T2-weighted images. Radiology 215 (3), 824–830.
Preziosa, P., Martinelli, V., Moiola, L., Radaelli, M., Gerevini, S., Guidetti, D., Immovilli, P., Michieletti, E., Scagnelli, P., Comola, M., Rocca, M.A., Filippi, M., Comi, G., 2016. Dynamic pattern of clinical and MRI findings in a tumefactive demyelinating lesion: a case report. J. Neurol. Sci. 361, 184–186. https://doi.org/10.1016/j.jns.2015.12.039.
Rangwala, N.A., Hackney, D.B., Dai, W., Alsop, D.C., 2013. Diffusion restriction in the human spinal cord characterized in vivo with high b-value STEAM diffusion imaging. Neuroimage 82, 416–425. https://doi.org/10.1016/j.neuroimage.2013.05.122.
Rocca, M.A., Horsfield, M.A., Sala, S., Copetti, M., Valsasina, P., Mesaros, S., Martinelli, V., Caputo, D., Stosic-Opincal, T., Drulovic, J., Comi, G., Filippi, M., 2011. A multicenter assessment of cervical cord atrophy among MS clinical phenotypes. Neurology 76 (24), 2096–2102. https://doi.org/10.1212/WNL.0b013e31821f46b8.
Rovira, A., Pericot, I., Alonso, J., Rio, J., Grivé, E., Montalban, X., 2002. Serial diffusion-weighted MR imaging and proton MR spectroscopy of acute large demyelinating brain lesions: case report. Am. J. Neuroradiol. 23, 989–994. https://doi.org/10.1038/nrn3516.
Sapkota, Nabraj, Shi, X., Shah, L.M., Bisson, E.F., Rose, J.W., Jeong, E.K., 2016a. Two-dimensional single-shot diffusion-weighted stimulated EPI with reduced FOV for ultrahigh-b radial diffusion-weighted imaging of spinal cord. Magn. Reson. Med. https://doi.org/10.1002/mrm.26302.
Sapkota, N., Thapa, B., Lee, YouJung, Kim, T., Bisson, E.F., Shah, L.M., Rose, J.W., Jeong, E.-K., 2016b. Eight-channel decoupled array for cervical spinal cord imaging at 3T: six-channel posterior and two-channel anterior array coil. Concepts Magn. Reson. Part B Magn. Reson. Eng. 46B (2), 90–99. https://doi.org/10.1002/cmr.b.2016.46B.issue-210.1002/cmr.b.21325.
Sapkota, N., Yoon, S., Thapa, B., Lee, Y., Bisson, E., Bowman, B., Miller, S., Shah, L., Rose, J., Jeong, E., 2016. Characterization of spinal cord white matter by suppressing signal from hindered space. A Monte Carlo simulation and an ex vivo ultrahigh-b diffusion-weighted imaging study. J. Magn. Reson. 272, 53–59. https://doi.org/10.1016/j.jmr.2016.09.001.
Schmierer, K., Scaravilli, F., Altmann, D.R., Barker, G.J., Miller, D.H., 2004. Magnetization transfer ratio and myelin in postmortem multiple sclerosis brain. Ann. Neurol. 56 (3), 407–415. https://doi.org/10.1002/(ISSN)1531-824910.1002/ana.v56:310.1002/ana.20202.
Smith, A.K., Dortch, R.D., Dethrage, L.M., Smith, S.A., 2014. Rapid, high-resolution quantitative magnetization transfer MRI of the human spinal cord. Neuroimage 95, 106–116.
Soellinger, M., Langkammer, C., Seifert-Held, T., Fazekas, F., Ropele, S., 2011. Fast bound pool fraction mapping using stimulated echoes. Magn. Reson. Med. 66 (3), 717–724. https://doi.org/10.1002/mrm.22846.
Thapa, B., Sapkota, N., Lee, YouJung, Jeong, K., Rose, J., Shah, L.M., Bisson, E., Jeong, E.-K., 2018. Ultra-high-b radial diffusion-weighted imaging (UHb-rDWI) of human cervical spinal cord. J. Magn. Reson. Imaging 49 (1), 204–211. https://doi.org/10.1002/jmri.v49.110.1002/jmri.26169.
Thompson, A.J., Kermode, A.G., Wicks, D., MacManus, D.G., Kendall, B.E., Kingsley, D.P. E., McDonald, W.I., 1991. Major differences in the dynamics of primary and secondary progressive multiple sclerosis. Ann. Neurol. 29 (1), 53–62. https://doi.org/10.1002/ana.v29:110.1002/ana.410290111.
Yoshiura, T., Wu, O., Zaheer, A., Reese, T.G., Gregory Sorensen, A., 2001. Highly diffusion-sensitized MRI of brain: dissociation of gray and white matter. Magn. Reson. Med. 45, 734–740. https://doi.org/10.1002/mrm.1100.